Research in Astron. Astrophys. **2012** Vol. **12** No. **5**, 485–499
*http://www.raa-journal.org* *http://www.iop.org/journals/raa*

***R**esearch in*
***A**stronomy and*
***A**strophysics*

# Peculiar early-type galaxies with central star formation *

Chong Ge[1] and Qiu-Sheng Gu[1,2]

[1] School of Astronomy and Space Science, Nanjing University, Nanjing 210093, China; *chongge.nju@gmail.com*
[2] Key Laboratory of Modern Astronomy and Astrophysics, Nanjing University, Ministry of Education, Nanjing 210093, China

Received 2011 October 10; accepted 2012 January 13

**Abstract** Early-type galaxies (ETGs) are very important for understanding the formation and evolution of galaxies. Recent observations suggest that ETGs are not simply old stellar spheroids as we previously thought. Widespread recent star formation, cool gas and dust have been detected in a substantial fraction of ETGs. We make use of the radial profiles of $g-r$ color and the concentration index from the Sloan Digital Sky Survey database to pick out 31 peculiar ETGs with central blue cores. By analyzing the photometric and spectroscopic data, we suggest that the blue cores are caused by star formation activities rather than the central weak active galactic nucleus. From the results of stellar population synthesis, we find that the stellar population of the blue cores is relatively young, spreading from several Myr to less than one Gyr. In 14 galaxies with H I observations, we find that the average gas fraction of these galaxies is about 0.55. The bluer galaxies show a higher gas fraction, and the total star formation rate (SFR) correlates very well with the H I gas mass. The star formation history of these ETGs is affected by the environment, e.g. in the denser environment the H I gas is less and the total SFR is lower. We also discuss the origin of the central star formation of these early-type galaxies.

**Key words:** galaxies: elliptical and lenticular, cD — galaxies: peculiar — galaxies: evolution

## 1 INTRODUCTION

Early-type galaxies (ETGs), which dominate the stellar mass density in the local universe, are very important for understanding the formation and evolution of galaxies (Bernardi et al. 2003). Early studies regarded ETGs as simple systems, with a smooth morphology, an old stellar population, a red optical color, free of cold gas and having ongoing star formation (Searle et al. 1973; Larson 1974). In particular, ETGs obey some optical scaling relations, such as the fundamental plane, e.g. the tight relationship among half-light radius ($r_{50}$), half-light surface brightness ($I_{50}$) and velocity dispersion ($\sigma$) (e.g. Djorgovski & Davis 1987; Faber et al. 1987; Jorgensen et al. 1996); and the color-magnitude relation (Sandage & Visvanathan 1978), with brighter galaxies being redder. The small scatter in this relationship requires the stellar content of the ETGs to be fairly uniform and

* Supported by the National Natural Science Foundation of China.

predominantly old (Bower et al. 1992). Traditionally, we have regarded ETGs as "red and passive" galaxies, based on optical observations.

However, recent multi-wavelength observations point out that ETGs show a wide range of diversity in their stellar population, and they are not as simple as we previously thought. Early results from the Galaxy Evolution Explorer (*GALEX*) suggested that some optically red ETGs show strong UV excess (Yi et al. 2005). Fukugita et al. (2004) reported four star-forming ETGs from the Sloan Digital Sky Survey (SDSS) Data Release 2, where the star formation rates (SFRs) can be comparable with those found in normal spiral galaxies. With a much larger sample of 16 000 ETGs, Schawinski et al. (2007a) found that about four percent of ETGs show emission lines characteristic of ongoing star formation. However, the fraction of these active elliptical or ETGs actually highly depends on the data and the galaxy's stellar mass (see Schawinski et al. 2006; Schawinski et al. 2007b). More recently, Huang & Gu (2009) reported 13 ETGs showing unambiguous evidence of recent star formation activity portrayed by conspicuous nebular emission lines, and suggested that the star formation history of ETGs can be well described by a recent minor and short starburst superimposed on an old stellar component. Moreover, H I gas, molecular gas and warm dust have also been detected in a significant fraction of ETGs (e.g. Morganti et al. 2006; Combes et al. 2007; Oosterloo et al. 2010; Smith et al. 2011; the SAURON project, Bacon et al. 2001; the ATLAS$^{3D}$ project, Cappellari et al. 2011). However, there still remain several important issues, such as the time-scale and intensity of the recent star formation, and their triggering mechanism to constrain the ETG's formation scenario.

Gu et al. (2006) discovered an elliptical galaxy, IC 225, with a peculiar blue core. Lisker et al. (2006) identified some early-type dwarfs with central blue colors caused by recent or ongoing star formation in the Virgo Cluster. These peculiar ETGs still form new stars in the central region. In this study, following Gu et al. (2006), we pick out more peculiar ETGs with blue cores from the Third Reference Catalog of Bright Galaxies (RC3, de Vaucouleurs et al. 1995), and mainly use SDSS Data Release 7 data (Abazajian et al. 2009). There are two possible ways to cause these blue cores in SDSS optical images: (1) a power-law continuum from the central active galactic nucleus (AGN); and (2) star formation activities. With this large sample of ETGs having blue cores, we investigate their photometric and spectroscopic properties, stellar population, gas content and environment, and we also discuss the formation scenario of the blue cores in these peculiar galaxies.

## 2 SAMPLE

There are several methods to classify galaxies into different morphological types, such as the concentration index, the "fracDev" parameter[1] in SDSS, and the Sersic index. We first select ETGs with a regular morphological shape and a blue inner region by visual inspection of 23 011 galaxies in the RC3 catalog. Then we use other parameters to double-check the sample galaxies further in the following way.

(1) We use the concentration index ($C_r$, defined as the ratio of the radii containing 90 percent and 50 percent of the Petrosian $r$ band light) to clarify whether these galaxies are really ETGs. The $r$-band Petrosian radii, $r_{50}$ and $r_{90}$, are extracted from the SDSS database. The concentration index is well correlated with galaxy type; for an ideal de Vaucouleurs profile, $C_r \sim 5.5$, while for an exponential disk, $C_r \sim 2.3$. In this paper, we select the ETGs with $C_r > 2.6$ (Strateva et al. 2001).
(2) We use the radial color profile to clarify whether these galaxies contain a blue core. We take advantage of SDSS $g$- and $r$-band images, and match the point spread function (PSF) of these two

[1] The SDSS outputs the exponential and de Vaucouleurs profile fits for $u-$, $g-$, $r-$, $i-$ and $z-$band images and asks for the linear combination of the two that best fits the image. The coefficient of the de Vaucouleurs term is stored as fracDeV. fracDeV = 1 means a pure de Vaucouleurs profile; fracDeV = 0 means a pure exponential profile.

different band images; then we make use of the "ellipse" in *IRAF*[2] to get the surface brightness distribution.

(3) In order to study the nature of the blue core in ETGs, we restrict our sample to cases having an SDSS spectrum. Finally, we get a sample of 31 ETGs with blue cores, which will be abbreviated as ETG(bc)s hereafter.

Figure 1 shows the $u-$, $g-$ and $r-$band multi-color images, and the radial $g-r$ color profiles after matching the point spread function (PSF) of the $g-$ and $r-$band images with each of the three ETG(bc)s in our sample. Table 1 presents the basic properties of our ETGs showing central blue cores.

## 3 DATA ANALYSES

### 3.1 Stellar Population Synthesis

In order to explore the stellar population of ETG(bc)s, we apply the stellar population synthesis code, STARLIGHT[3] (Cid Fernandes et al. 2005; Mateus et al. 2006; Asari et al. 2007; Cid Fernandes et al. 2007), which fits an observed spectrum ($O_\lambda$) with a linear combination of 45 simple stellar populations (SSPs) from the evolutionary synthesis model of BC03 (Bruzual & Charlot 2003). The model spectrum is given by

$$M_\lambda = M_{\lambda 0}\left(\sum_{j=1}^{N_\star} x_j b_{j,\lambda} r_\lambda\right) \otimes G(v_\star, \sigma_\star), \quad (1)$$

where $M_\lambda$ is the model spectrum, $M_{\lambda 0}$ is the synthesis flux at the normalization wavelength, $x_j$ is the population vector, representing the fractional contribution of the $j$th SSP, $b_{j,\lambda}$ is $j$th SSP spectrum at $\lambda$, $r_\lambda \equiv 10^{0.4(A_\lambda - A_{\lambda 0})}$ is the reddening term, and $G(v_\star, \sigma_\star)$ is the line-of-sight stellar motions modeled by a Gaussian distribution centered at velocity $v_\star$ with velocity dispersion $\sigma_\star$. $N_\star = 45$ SSPs-15 ages ($t = 0.001$, 0.00316, 0.00501, 0.01, 0.02512, 0.04, 0.10152, 0.28612, 0.64054, 0.90479, 1.434, 2.5, 5, 11 and 13 Gyr) and three metallicities ($Z = 0.2$, 1 and 2.5 $Z_\odot$); their spectra were computed with the Chabrier (2003) IMF, STELIB library (Le Borgne et al. 2003) and Padova-2004 models. The intrinsic extinction is modeled due to foreground dust and parameterized by the $V$-band extinction, $A_V$, using the extinction law of Cardelli et al. (1989) with $R_V = 3.1$.

Before fitting, the spectra are corrected for the galactic extinction using the maps of Schlegel et al. (1998) and applying the Cardelli et al. (1989) extinction law, shifted to the rest frame; then they are rebinned by 1 Å from 3800 to 8600 Å; the spectral regions of strong emission lines, bad pixels and sky residuals are masked out during the fitting. The best-fitting population is found by searching for the minimum $\chi^2 = \sum_\lambda [(O_\lambda - M_\lambda) w_\lambda]^2$, where $w_\lambda^{-1}$ is the error in $O_\lambda$.

Figure 2 shows an example of the spectral fit for IC 692 in our sample. The top panel shows the observed spectrum (black) and the fitting (red), and the bottom panel shows the residual spectrum ($O_\lambda - M_\lambda$, black) and the masked spectral regions (red).

### 3.2 Mean Stellar Age and Metallicity

STARLIGHT shows the fractional contribution weighted by light and the stellar mass of each SSP. Following Cid Fernandes et al. (2005), we choose the light-weighted mean stellar age to characterize

[2] The "ellipse" task fits elliptical isophotes to galaxy images and calculates a mean intensity and error at different radii. We divide the mean intensities at the same radius of two band images to derive the radial color profiles. *IRAF* is distributed by the National Optical Astronomy Observatories, which is operated by the Association of Universities for Research in Astronomy, Inc., under cooperative agreement with the National Science Foundation.

[3] *http://www.starlight.usfc.br/*

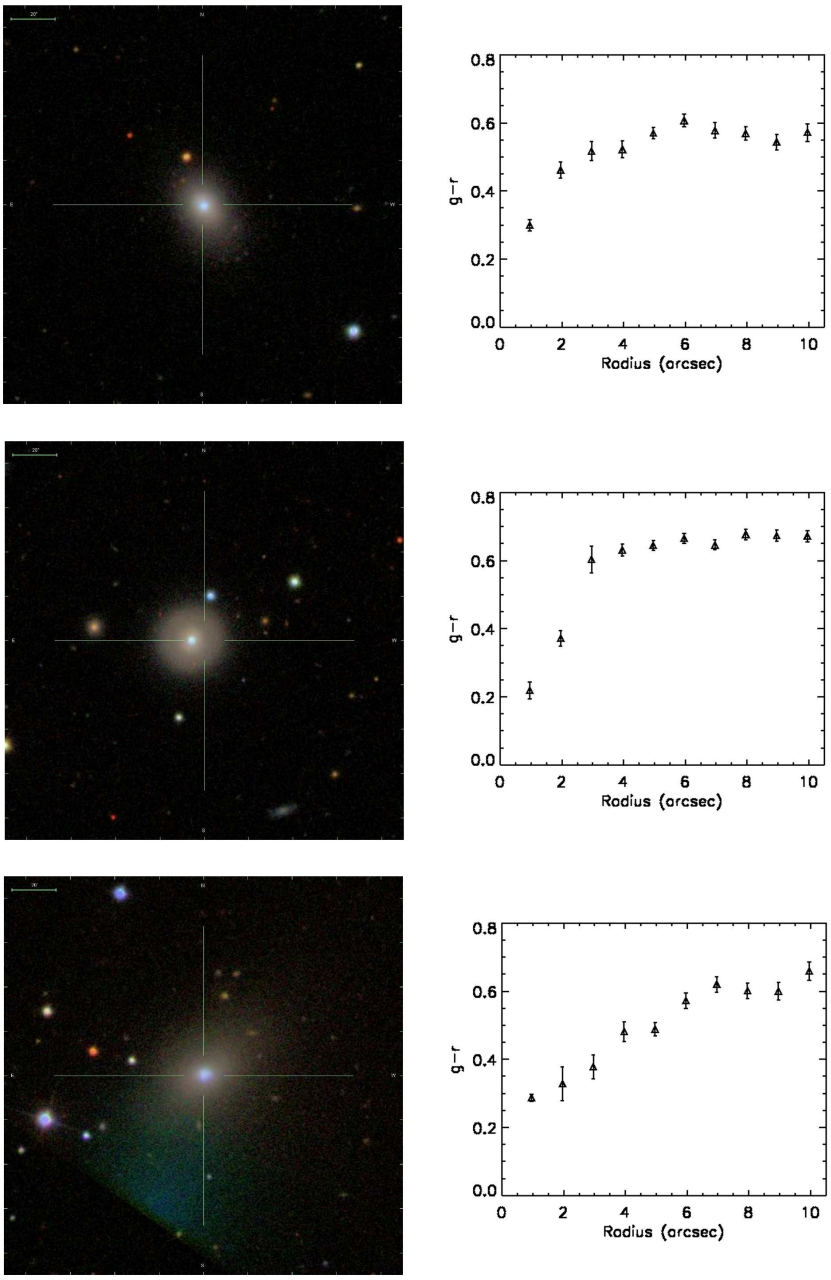


**Fig. 1** SDSS $u-$, $g-$ and $r-$band multi-color images and the radial $g-r$ color profiles for three ETG(bc)s in our sample. The color gradient is positive. Error bars are calculated by the "ellipse" task in *IRAF*. From top to bottom are PGC 43121 (3.01), PGC 49927 (2.58) and UGC 5179 (2.63), respectively. The number in brackets is the concentration index ($r_{90}/r_{50}$). These ETGs show a blue core with a typical elliptical profile (*color online*).

**Table 1** Early-Type Galaxies with Blue Cores

| SDSS id/NAME | $\alpha$ (J2000.0) (h m s) | $\delta$ (J2000.0) (° ′ ″) | Dist. (Mpc) | $r_{\rm fiber}$ (pc) | $r_{50}$ (pc) | ratio | $C_r$ | $M_r$ |
|---|---|---|---|---|---|---|---|---|
| (1) | (2) | (3) | (4) | (5) | (6) | (7) | (8) | (9) |
| SDSS J022628.28+010937.7/IC 225 | 02 26 28.3 | +01 09 38 | 17.7 | 129 | 814 | 0.16 | 2.63 | −17.28 |
| SDSS J082938.74+520434.8/PGC 23834 | 08 29 38.7 | +52 04 35 | 25.8 | 188 | 410 | 0.46 | 3.03 | −17.47 |
| SDSS J091645.52+532634.6/PGC 26188 | 09 16 45.5 | +53 26 35 | 32.8 | 239 | 544 | 0.44 | 2.71 | −17.92 |
| SDSS J093922.38+363428.4/PGC 27539 | 09 39 22.4 | +36 34 29 | 85.3 | 621 | 1989 | 0.31 | 3.02 | −19.71 |
| SDSS J094301.64+585824.9/UGC 5179 | 09 43 01.6 | +58 58 25 | 20.5 | 149 | 1074 | 0.14 | 2.63 | −17.39 |
| SDSS J094804.68+325257.0/PGC 28169 | 09 48 04.7 | +32 52 57 | 24.5 | 178 | 457 | 0.39 | 2.89 | −17.65 |
| SDSS J095732.85+333711.0/IC 2524 | 09 57 32.8 | +33 37 11 | 23.5 | 171 | 452 | 0.38 | 3.05 | −17.55 |
| SDSS J095836.23+131518.9/PGC 28817 | 09 58 36.2 | +13 15 19 | 51.9 | 378 | 1281 | 0.29 | 2.98 | −19.34 |
| SDSS J101628.22+451917.6/PGC 30005 | 10 16 28.2 | +45 19 18 | 25.7 | 187 | 460 | 0.41 | 2.75 | −17.41 |
| SDSS J102949.28+161051.2/PGC 30932 | 10 29 49.3 | +16 10 51 | 48.4 | 352 | 820 | 0.43 | 3.27 | −18.17 |
| SDSS J103837.25+443123.0/PGC 31639 | 10 38 37.2 | +44 31 23 | 53.8 | 391 | 747 | 0.52 | 2.95 | −19.06 |
| SDSS J104214.22+474600.2/PGC 31888 | 10 42 14.2 | +47 46 00 | 23.9 | 174 | 550 | 0.32 | 2.84 | −16.93 |
| SDSS J111836.34+631650.2/PGC 34582 | 11 18 36.3 | +63 16 50 | 46.0 | 335 | 907 | 0.37 | 3.07 | −19.17 |
| SDSS J112553.46+095914.9/IC 692 | 11 25 53.5 | +09 59 15 | 20.7 | 151 | 598 | 0.25 | 2.77 | −17.78 |
| SDSS J113028.60+480638.6/PGC 35467 | 11 30 28.6 | +48 06 39 | 116.4 | 847 | 1267 | 0.67 | 2.80 | −19.38 |
| SDSS J113536.39+155830.1/PGC 35838 | 11 35 36.4 | +15 58 30 | 76.6 | 557 | 849 | 0.66 | 3.03 | −18.69 |
| SDSS J114332.72+312728.4/PGC 36418 | 11 43 32.7 | +31 27 28 | 28.8 | 210 | 510 | 0.41 | 2.60 | −17.36 |
| SDSS J114556.60+501159.0/NGC 3870 | 11 45 56.6 | +50 11 59 | 13.1 | 95 | 401 | 0.24 | 2.73 | −17.57 |
| SDSS J114700.72−001739.2/PGC 36750 | 11 47 00.7 | −00 17 39 | 25.2 | 183 | 821 | 0.22 | 2.60 | −17.44 |
| SDSS J120515.83+305120.2/PGC 38277 | 12 05 15.8 | +30 51 20 | 11.84 | 86 | 342 | 0.25 | 2.85 | −16.00 |
| SDSS J121035.68+114538.9/PGC 38747 | 12 10 35.7 | +11 45 39 | 22.4 | 163 | 469 | 0.35 | 2.68 | −16.83 |
| SDSS J122417.04+672623.9/PGC 40349 | 12 24 17.0 | +67 26 24 | 19.3 | 140 | 451 | 0.31 | 3.08 | −17.10 |
| SDSS J123233.50+091025.1/PGC 41587 | 12 32 33.5 | +09 10 25 | 20.4 | 148 | 424 | 0.35 | 2.91 | −17.14 |
| SDSS J124655.40+263351.3/PGC 43121 | 12 46 55.4 | +26 33 51 | 14.8 | 108 | 391 | 0.28 | 3.01 | −16.51 |
| SDSS J124841.02+342839.3/PGC 43281 | 12 48 41.0 | +34 28 39 | 61.6 | 448 | 973 | 0.46 | 3.18 | −19.40 |
| SDSS J130034.91+642649.6/PGC 44782 | 13 00 34.9 | +64 26 50 | 29.9 | 218 | 820 | 0.27 | 2.80 | −17.48 |
| SDSS J130604.02+532943.1/PGC 45337 | 13 06 04.0 | +53 29 43 | 100.9 | 734 | 1413 | 0.52 | 2.92 | −19.61 |
| SDSS J132000.98+520303.2/PGC 46505 | 13 20 01.0 | +52 03 03 | 65.4 | 476 | 761 | 0.63 | 2.82 | −18.70 |
| SDSS J132420.16+363545.9/PGC 46854 | 13 24 20.2 | +36 35 46 | 69.1 | 503 | 1220 | 0.41 | 2.87 | −19.81 |
| SDSS J140124.02+364800.3/PGC 49927 | 14 01 24.0 | +36 48 00 | 39.7 | 289 | 1239 | 0.23 | 2.58 | −19.03 |
| SDSS J141842.39+245519.8/PGC 214248 | 14 18 42.4 | +24 55 20 | 64.3 | 468 | 1155 | 0.40 | 2.72 | −18.33 |

Notes: List of ETG(bc)s and their parameters. Columns: (1) galaxy SDSS id and corresponding RC3 catalog name; (2−3) right ascension and declination at epoch J2000; (4) distance from NED in Mpc; (5) physical galaxy radius covered by SDSS fiber in pc, calculated by multiplying the SDSS $1.5''$ fiber radius by the galaxy's distance in column (4); (6) $r$-band half-light radius in pc; (7) the ratio between $r_{\rm fiber}$ and $r_{50}$; (8) the concentration index; (9) $r$-band absolute magnitude.

the stellar population mixture of a galaxy, which is more sensitive to the young stellar population and the residual star formation activity.

$$\langle \log t_\star \rangle_L = \sum_{j=1}^{N_\star} x_j \log t_j, \tag{2}$$

where $x_j$ is the fraction of flux contributed by the $j$th SSP. The light-weighted mean metallicity ($\langle Z_\star \rangle_L$) is calculated in the same way.

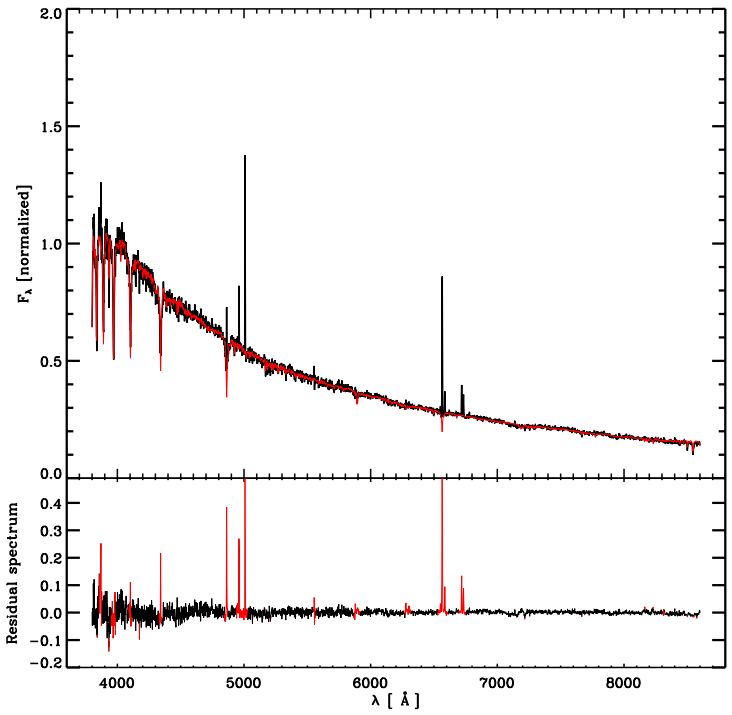


**Fig. 2** Spectral synthesis of the galaxy (IC 692) in our sample. *Top panel*: observed (*thick black line*) and model (*thin red line*) spectra (*color online*). *Bottom panel*: the residual spectrum (*black*) and the masked regions (*red*).

## 4 RESULTS

### 4.1 Spectroscopic Properties

The SDSS spectrum comes from a single fiber, which has a wavelength coverage of 3800–9200 Å and a resolution of about 1800. The fiber radius corresponds to an angular size of $1.5''$, and this fixed aperture corresponds to a different physical size at different distances. So the spectrum is a nuclear spectrum for the nearby galaxies and a global spectrum for the distant galaxies.

Table 1 shows the corresponding physical size (Col.(5)) and a ratio (Col.(7)) of this physical size to the half-light radius (Col.(6)). From column (7) of Table 1, we find that the ratio is small, so our spectral properties are for the very central region of these galaxies.

After removing the contribution from the old stellar population, we can derive the pure emission-line spectrum, where we can measure the accurate emission line fluxes, such as H$\beta$, [O III]$\lambda$5007, H$\alpha$, [N II]$\lambda$6583 and [S II]$\lambda$6716, 6731.

Figure 3 shows the BPT diagram (Baldwin et al. 1981) of these ETG(bc)s. Detailed photoionization modeling (Osterbrock 1989) showed that the optical line ratio, [O III]$\lambda$5007/H$\beta$, is a good indicator of the mean level of ionization and the temperature of the emitting gas, while [N II]$\lambda$6583/H$\alpha$ is sensitive to the size of the partially ionized zone produced by high-energy photoionization, both of which are higher in AGNs. According to the line ratio, the BPT diagram can be roughly divided into three regions (following Kauffmann et al. 2003b) to separate star-forming galaxies from AGNs. From the BPT diagram, we find that all the ETG(bc)s belong to star-forming galaxies, which rules out the possibility of AGN activity causing the blue core. In fact, the radiation area of the AGN

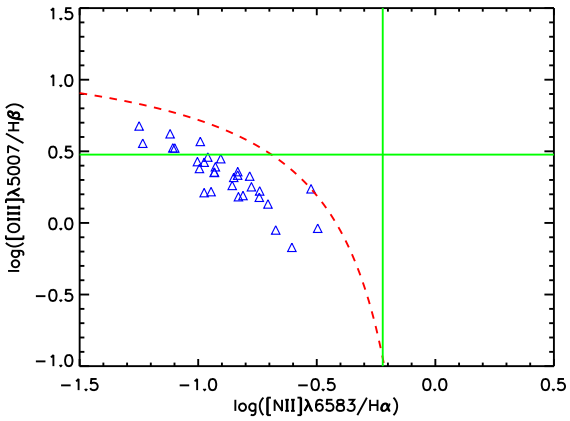


**Fig. 3** Emission-line flux ratio [O III]$\lambda$5007/H$\beta$ versus [N II]$\lambda$6583/H$\alpha$ for the ETG(bc)s; this diagram is also called the BPT diagnostic diagram. Divisions are based on Kauffmann et al. (2003a) to distinguish star-forming galaxies, LINERs and Seyferts. The dashed line represents the demarcation line of pure star formation. Seyfert galaxies have [O III]$\lambda$5007/H$\beta$ >3 and [N II]$\lambda$6583/H$\alpha$ >0.6. LINERs have [O III]$\lambda$5007/H$\beta$ <3 and [N II]$\lambda$6583/H$\alpha$ >0.6. All our ETG(bc)s are star-forming galaxies.

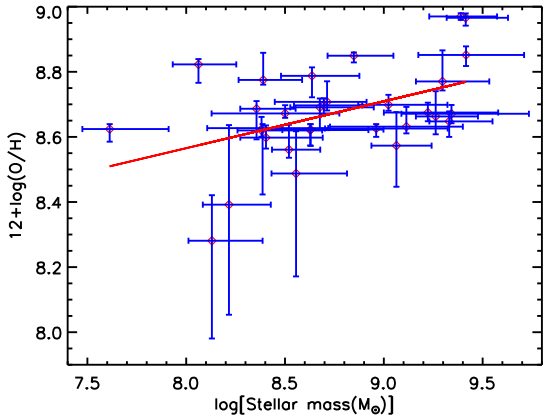


**Fig. 4** The stellar mass and gas-phase metallicity relation of ETG(bc)s. The stellar mass is based on Kauffmann et al. (2003a) and Salim et al. (2007); the gas-phase metallicity is from Tremonti et al. (2004). The diamonds are the median values of bayesian likelihood estimates for the parameters, and the error bars are the 2.5 and 97.5 percentile ranges of the probability distribution. The line is the linear least squares fit, and the correlation coefficient is equal to 0.47. More massive ETG(bc)s tend to have a slightly higher metallicity.

is very small, and the AGN cannot affect the color to a radius significantly larger than the seeing, typically $1.4''$ in the SDSS $r$-band. From the radial color profile in Figure 1, we find that the blue core region is larger than $1.4''$, so the outer region of the blue core must be caused by star formation activities. The result from the BPT digram confirms that the inner region of the blue core is caused by star formation activities.

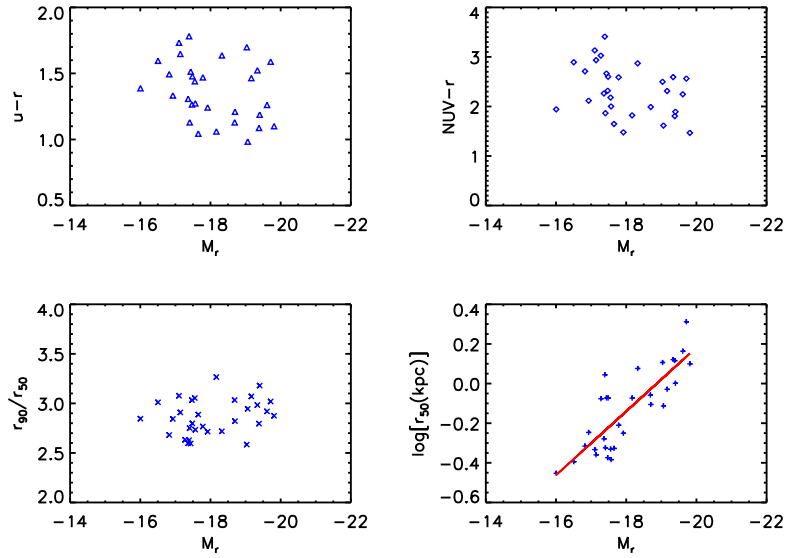


**Fig. 5** Distribution of photometric properties of ETG(bc)s from SDSS and *GALEX*. *Top left*: CMR of $u-r$ color with $r$-band absolute Petrosian magnitude ($M_r$). *Top right*: CMR of $NUV-r$ color with $M_r$. *Bottom left*: the concentration index vs. $M_r$. *Bottom right*: $r_{50}$ (effective radius) vs. $M_r$; the solid line is the linear least squares fit, and the scaling relation is $r_{50} \propto L^{0.40}$.

Figure 4 shows the stellar mass-metallicity relation for these ETG(bc)s. The stellar mass is based on fitting to the photometry following Kauffmann et al. (2003a) and Salim et al. (2007). The gas-phase metallicity is represented by the oxygen abundance and by following Tremonti et al. (2004). The relatively high gas-phase metallicity of our sample, compared with the Sun ($\langle 12+\log(\mathrm{O/H})\rangle = 8.69$), rules out the possibility of an external origin of gas through accretion processes from the low metallicity intergalactic medium (IGM). The correlation coefficient between the stellar mass and the gas-phase metallicity is 0.47. There is a tendency that more massive ETG(bc)s have slightly higher metallicity, which is the same as star-forming spiral galaxies (Tremonti et al. 2004). Moreover, the masses of these ETG(bc)s are relatively low, which will be discussed below.

### 4.2 Photometric Properties

Figure 5 shows the general photometric properties of ETG(bc)s from the SDSS and *GALEX* data: the $u-r$ color, the $NUV-r$ color, the concentration index and the physical half-light radius ($r_{50}$, also called the effective radius) with the relation to the $r$-band absolute Petrosian magnitude ($M_r$).

The top left panel of Figure 5 shows the color-magnitude relation (CMR) of $u-r$ Petrosian color versus $M_r$, where the colors have already been corrected for galactic extinction (Schlegel et al. 1998). The most well-known feature in the CMR is a bimodal color distribution of galaxies (Strateva et al. 2001; Blanton et al. 2003; Baldry et al. 2004). Generally, galaxies can be divided into red sequence (massive early-type passive galaxies) and blue cloud (galaxies with active star formation) cases. From the CMR, we find that all the ETG(bc)s belong to the blue cloud region according to $u-r < 2.22$ (Strateva et al. 2001). However, normal ETGs tend to be located in the red sequence due to their predominantly old stellar content. These peculiar ETG(bc)s are located in the blue cloud because they harbor star-forming activities, which make them different from normal ETGs.

The top right panel of Figure 5 shows $NUV-r$ color with $M_r$. The NUV magnitude of our sample is from *GALEX*. Star formation activities will produce UV excess, so these ETG(bc)s will

be bluer in UV. However, another UV excess could arise from old, extreme horizontal branch (HB) stars, that leads to the "UV upturn" phenomenon around 1500 Å (e.g. Yi et al. 1999). Kaviraj et al. (2007), using the $NUV-r$ color, found that objects with $NUV-r \leq 5.4$ are highly likely to harbor recent star formation instead of the UV excess from the old stars. From the CMR of $NUV-r$ with $M_r$, all ETG(bc)s have $NUV-r \leq 4$, which supports the blue cores being caused by star formation activities.

From the bottom left of Figure 5, we find that the concentration index of ETG(bc)s lies between 2.6 and 3.3, closer to the concentration index of the exponential disk profile ($C_r$ ∼2.3) than the de Vaucouleurs profile ($C_r$ ∼5.5), so these ETG(bc)s are more likely to be exponential disk galaxies whose stellar component is not completely relaxed yet.

The bottom right panel of Figure 5 shows the relation of effective radius with $M_r$. The solid line is the linear least squares fit and the two parameters correlate well, with the correlation coefficient equal to –0.83. (The $x$-axis is reversed, from left to right; the galaxy magnitude is progressively smaller, and the galaxy is progressively more luminous). The more luminous galaxies have larger optically emitting regions, and the scaling relation is $r_{50} \propto L^{0.40}$.

### 4.3 Stellar Population

By analyzing the photometric and spectroscopic data in Sections 4.1 and 4.2, we suggest that the most probable origin of the blue cores in ETGs is caused by recent star-formation activities, rather than AGN activities.

Figure 6 shows the distribution of light-weighted properties in the age-metallicity plane from the results of stellar population synthesis. The light-weighted properties are calculated by Equation (2), and we use flux weighted mean stellar age to characterize the stellar population mixture of a galaxy, so they are more sensitive to the young stellar population and the residual star formation activities. The dotted and dashed lines respectively represent the average stellar population age and metallicity of the sample. We find that the distribution of the stellar population in the blue cores of ETG(bc)s is relatively young compared with normal ETGs but with quite large scatter. Some of the stellar population is very young, around several Myr, but some is relatively old, perhaps slightly less than one Gyr. This result confirms that ongoing or very recent star formation takes place at the center of these ETGs.

## 5 GAS AND ENVIRONMENT

### 5.1 Gas Fraction

From the results of BPT, CMR and stellar population synthesis presented above, we find that these ETG(bc)s embrace either ongoing or very recent star formation, so there must be a certain amount of gas to fuel the star formation.

From the HyperLeda Database[4] (Paturel et al. 2003), and the NASA/IPAC Extragalactic Database (NED), we obtain 21 cm line flux data for 14 ETG(bc)s. We convert them to H I mass using equation $M_{\rm HI} = 2.356 \times 10^5 D^2 f_{\rm 21cm}$, where $D$ is the distance in Mpc, and $f_{\rm 21cm}$ is the 21-cm line flux in Jy km s$^{-1}$ (eq. (9), Haynes & Giovanelli 1984). Then we investigate the ratio between the total gas mass and the total baryonic mass in the ETG(bc)s. The gas fraction is defined as $f_{\rm gas} = M_{\rm gas}/(M_{\rm gas} + M_{\rm star})$ following Geha et al. (2006), where the total gas mass is $M_{\rm gas} = 1.4 M_{\rm HI}$, mainly including the mass of the H I and helium gas. We present the distribution of the gas fraction ($f_{\rm gas}$) with the stellar mass in Figure 7. Geha et al. (2006) found that there was a tendency for less massive galaxies to have higher gas fractions. In Figure 7 this tendency is not obviously limited to the size of our sample. The average gas fraction in our sample is around 0.55, which

[4] *http://leda.univ-lyon1.fr/*

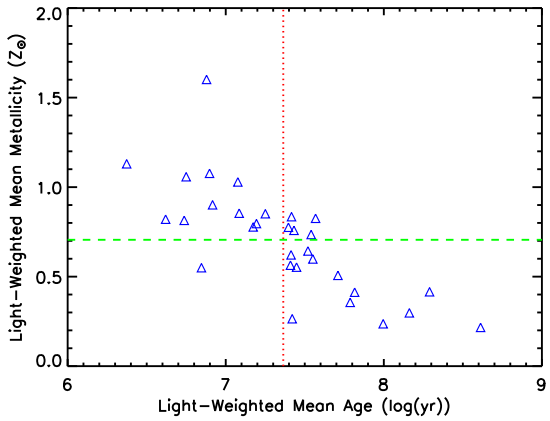


**Fig. 6** Distribution of the light-weighted mean age and metallicity of the ETG(bs)s from the result of spectral synthesis code STARLIGHT. The dotted red and dashed green lines respectively represent the average stellar population age and metallicity of the sample (*color online*). The stellar population of the blue core is relatively young but with quite large scatter.

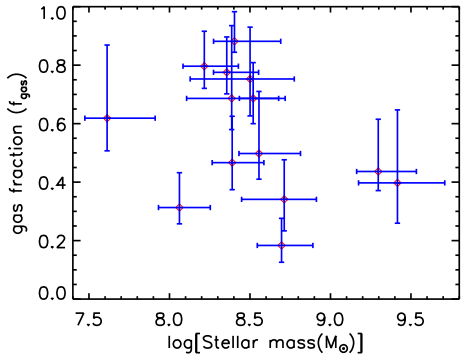


**Fig. 7** Gas fraction, $f_{\rm gas} = M_{\rm gas}/(M_{\rm gas} + M_{\rm star})$, plotted vs. stellar mass, and total gas mass $M_{\rm gas} = 1.4M_{\rm HI}$, mainly including the mass of the H I and helium gas. The average gas fraction is 0.55.

is very high compared with normal ETGs. However, these H I fluxes are from single-dish measurements, e.g. Arecibo, GBT and Effelsberg radio telescopes, and the H I fluxes may be overestimated. Interferometric observations will be needed to derive an accurate H I measurement.

We find that there is an anti-correlation between $g-r$ color and gas fraction as shown in Figure 8; the correlation coefficient is equal to $-0.68$. This result suggests that the ETG(bc) with a higher gas fraction has a bluer color.

### 5.2 SFRs and H I

From the above investigation of gas fractions, we know that these ETG(bc)s contain lots of gas, and these ETG(bc)s also harbor star formation activities, so we will further explore the relation between the SFRs and the gas mass. We utilized the total SFRs after aperture correction based on Brinchmann et al. (2004). The SFR in SDSS fibers is calculated by H$\alpha$ flux, and the total SFR needs aperture

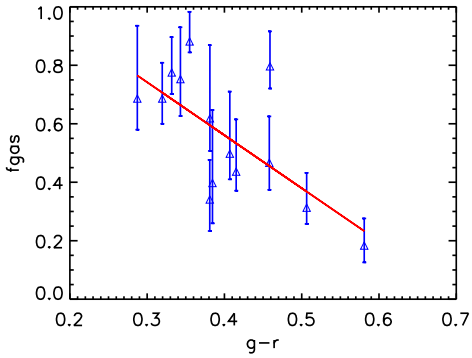


**Fig. 8** Gas fraction vs. $g-r$ color. The solid line is the linear least squares fit, and the correlation coefficient is equal to $-0.68$. The ETG(bc) with a higher gas fraction has a bluer color.

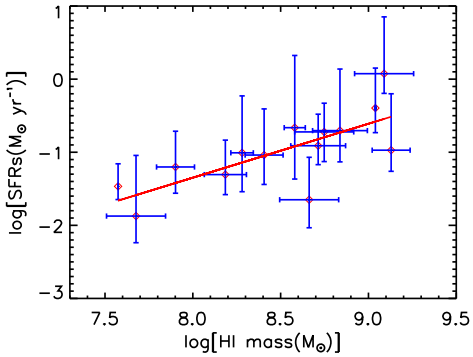


**Fig. 9** Relation between the total SFRs and the H I mass for 14 ETG(bc)s, the total SFRs after aperture correction are based on Brinchmann et al. (2004). The solid line is calculated by a linear least squares fit, and the correlation coefficient is 0.74. ETG(bc)s with more gas harbor higher SFRs.

correction according to the color of the galaxy. The results are shown in Figure 9. The solid line is the best fit by the linear least squares method. We find that the total SFR correlates well with the H I mass in these ETG(bc)s, with the correlation coefficient being 0.74. ETG(bc)s with more gas harbor higher SFRs.

### 5.3 Environmental Dependence

It is well known that the environment of a galaxy plays an important role in determining its properties, such as rest-frame color, star formation rate and gas content (Kauffmann et al. 2004; Baldry et al. 2006; Ellison et al. 2009). The most famous is the morphology-density relation found by Dressler (1980), who found that the fraction of spiral galaxies decreases with increasing local galaxy density in 55 nearby galaxy clusters, but the fraction of elliptical galaxies shows the opposite behavior. So we will explore the relationship between some of the properties of these ETG(bc)s with local galaxy density.

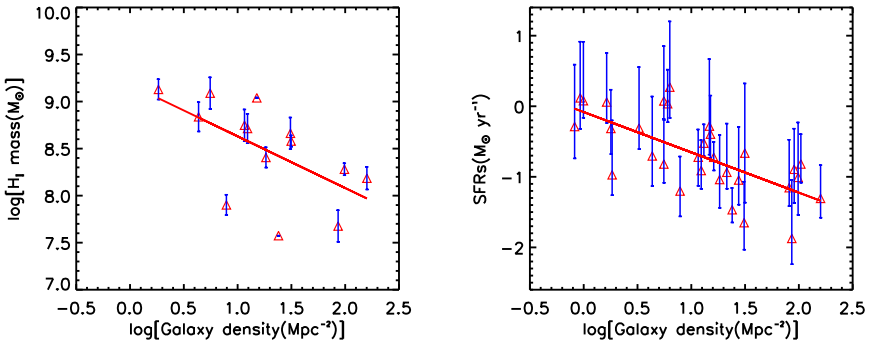


**Fig. 10** Distribution of galaxy properties with environment. *Left*: the relationship between the H I mass and the galaxy density; the correlation coefficient is $-0.59$. *Right*: the relationship between all the SFRs and the galaxy density; the correlation coefficient is $-0.69$. The lines in these figures are calculated by the linear least squares fit of the respective data.

To study the local density around each ETG(bc), we define

$$\Sigma_N = \frac{N}{\pi d_N^2}, \tag{3}$$

where $d_N$ is the projected distance to the $N$th nearest neighbor that is a member of the density defining population (DDP), within a reasonable redshift range. In this work, we choose $N = 5$ and a redshift range of $\pm$ 1000 km s$^{-1}$.

The left panel of Figure 10 shows the relation between the H I mass and the galaxy density of 14 ETG(bc)s with H I observations. The H I gas mass decreases with increasing local galaxy density, and the correlation coefficient is $-0.59$.

From Figure 9 we know that the SFRs correlate well with the H I mass. We plot the SFRs of 31 ETG(bc)s with galaxy density in the right panel of Figure 10. The SFRs also decrease with increasing local galaxy density and the correlation coefficient is $-0.69$. The trend is the same as the H I mass with the local galaxy density, as we expected, and this trend, where the star formation rates of galaxies or the star formation fraction decreases with increasing local galaxy density, is well established by many other works (Gómez et al. 2003; Kauffmann et al. 2004; Best 2004). Because the random velocities of the galaxies in a denser environment are generally larger, the time the two galaxies are close together is correspondingly shorter, and the chance that dynamical friction will leave them in a bound orbit is much reduced. So the star formation rates induced by interactions or mergers are reduced in a denser environment (Binney & Tremaine 1987).

## 6 DISCUSSION

We found that the ETG(bc)s in our sample were not very massive. The stellar mass of an ETG(bc) is around one billion solar masses. This result is consistent with a recent paper by Suh et al. (2011), who studied nine early-type galaxies with type II and Ib supernovae caused by recent star formation (RSF) activities, and found that SNe II/Ib preferentially occur in relatively small host galaxies ($M_r > -22$). In fact, most ETG(bc)s are dwarf galaxies. Dwarf elliptical galaxies tend to have less concentrated surface brightness profiles, which is consistent with the result from the concentration index. However, it is still not clear why blue cores tend to be embedded within low mass galaxies.

In the galaxy downsizing scenario (e.g. Fontanot et al. 2009), massive galaxies form earlier and then fade, so star formation starts at a lower redshift in lower mass galaxies. Low-mass galaxies, such as dwarf elliptical galaxies, are not effective in transforming cool gas into stars, which is probably

due to their low surface densities (Kennicutt 1998; Martin & Kennicutt 2001; Verde et al. 2002; Dalcanton et al. 2004). This is in accordance with the high gas fraction found in the ETG(bc)s. In lower mass galaxies, with a shallower halo potential well, the loss of metals through stellar winds and supernova (SN) ejecta becomes more important (Veilleux et al. 2005), which leads to the tendency we see in the mass-metallicity relation.

In the BPT diagram, we find that none of the ETG(bc)s in our sample show AGN activity, because most ETG(bc)s are dwarf galaxies. This result is consistent with Kauffmann et al. (2003b), who found that very few AGNs are found in galaxies with $M* < 10^{10} M_{\odot}$. From the relation between the mass of the central black holes and the mass of the host elliptical galaxies (Gültekin et al. 2009), we know that the central black holes in these galaxies are less massive, and their AGN activity should be very weak.

In addition to the mass dependence interpretation, another scenario is the environment dependence, e.g. the star formation activities in ETG(bc)s are induced by interactions or minor mergers. We have found a relation of decreasing SFRs in these ETG(bc)s with increasing local galaxy density. This is because, in a denser environment, the high relative velocities between galaxies makes the time the two galaxies are close together shorter, and so reduces the chance that dynamical friction will leave them in a bound orbit. So, the interactions or mergers are rarer in denser environments. However, if the star formation activities in the ETG(bc)s are caused by tidal interactions or minor mergers, the standard SDSS images may be too shallow to distinguish these faint tidal features.

## 7 CONCLUSION

We have presented a study of 31 early-type galaxies with blue cores, which are selected from the RC3 catalog based on the photometric and spectroscopic data of the SDSS. From the BPT diagram and CMR of $NUV - r$ with $M_r$, we find that the blue cores are caused by central star formation instead of AGN activity. From the results of stellar population synthesis, we find that the stellar population of the blue cores is relatively younger than normal ETGs, spreading from several Myr to less than one Gyr, and this is caused by ongoing or RSF activities. These ongoing or RSF activities also cause the ETG(bc)s shift to the blue cloud in the CMR of $u - r$ color with $M_r$, and the stellar component is not relaxed yet according to the concentration index. We find that the scaling relation between the effective radius and the luminosity is $r_{50} \propto L^{0.40}$.

From the H I observation, we find that the average gas fraction of these ETG(bc)s is 0.55, which is higher than the normal ETGs, and the bluer galaxies have a higher gas fraction. Their total SFRs correlate with the H I gas mass. The high gas-phase metallicity from the result of the mass-metallicity relation rules out the possibility of an external origin of gas through accretion processes. It is more probable that the gas has an internal origin.

The environment is very important to the evolution of ETG(bc)s, and we find a relation of decreasing gas mass and star formation rates with increasing local density.

**Acknowledgements** The authors are very grateful to the anonymous referee for his/her careful reading of the manuscript and instructive comments, which significantly improved the content of this paper. This work is supported by the Doctoral Fund of the Ministry of Education of China (20100091110009), the National Natural Science Foundation of China (Grant Nos. 10878010, 10221001 and 10633040) and the National Basic Research Program (973 Program, No. 2007CB815405). The STARLIGHT project is supported by the Brazilian agencies CNPq, CAPES and FAPESP and by the France-Brazil CAPES/Cofecub program. We acknowledge the use of the public data of the MPA-Garching/JHU DR7 catalog, and much of the exploratory work that led to the results contained in this paper benefited from an SQL database created by William Schoenell as part of the SEAGal project. Funding for the creation and distribution of the SDSS Archive has been provided by the Alfred P. Sloan Foundation, the participating institutions, the National Aeronautics and Space Administration, the National Science Foundation, the US

Department of Energy, the Japanese Monbukagakusho and the Max Planck Society. The SDSS web site is *http://www.sdss.org*. The SDSS is managed by the Astrophysical Research Consortium for the participating institutions. The participating institutions are The University of Chicago, Fermilab, the Institute for Advanced Study, the Japan Participation Group, Johns Hopkins University (JHU), Los Alamos National Laboratory, the Max Planck Institute for Astronomy (MPIA), the Max Planck Institute for Astrophysics (MPA), New Mexico State University, University of Pittsburgh, Princeton University, the United States Naval Observatory and the University of Washington. This research has made use of the NASA/IPAC Extragalactic Database, which is operated by the Jet Propulsion Laboratory, California Institute of Technology, under contract with the National Aeronautics and Space Administration. We acknowledge the usage of the HyperLeda database (*http://leda.univ-lyon1.fr*).

## References

Abazajian, K. N., Adelman-McCarthy, J. K., Agüeros, M. A., et al. 2009, ApJS, 182, 543
Asari, N. V., Cid Fernandes, R., Stasińska, G., et al. 2007, MNRAS, 381, 263
Bacon, R., Copin, Y., Monnet, G., et al. 2001, MNRAS, 326, 23
Baldry, I. K., Balogh, M. L., Bower, R. G., et al. 2006, MNRAS, 373, 469
Baldry, I. K., Glazebrook, K., Brinkmann, J., et al. 2004, ApJ, 600, 681
Baldwin, J. A., Phillips, M. M., & Terlevich, R. 1981, PASP, 93, 5
Bernardi, M., Sheth, R. K., Annis, J., et al. 2003, AJ, 125, 1817
Best, P. N. 2004, MNRAS, 351, 70
Binney, J., & Tremaine, S. 1987, Galactic Dynamics (Princeton, NJ: Princeton Univ. Press), 747
Blanton, M. R., Hogg, D. W., Bahcall, N. A., et al. 2003, ApJ, 594, 186
Bower, R. G., Lucey, J. R., & Ellis, R. S. 1992, MNRAS, 254, 601
Brinchmann, J., Charlot, S., White, S. D. M., et al. 2004, MNRAS, 351, 1151
Bruzual, G., & Charlot, S. 2003, MNRAS, 344, 1000
Cappellari, M., Emsellem, E., Krajnović, D., et al. 2011, MNRAS, 413, 813
Cardelli, J. A., Clayton, G. C., & Mathis, J. S. 1989, ApJ, 345, 245
Chabrier, G. 2003, PASP, 115, 763
Cid Fernandes, R., Asari, N. V., Sodré, L., et al. 2007, MNRAS, 375, L16
Cid Fernandes, R., Mateus, A., Sodré, L., Stasińska, G., & Gomes, J. M. 2005, MNRAS, 358, 363
Combes, F., Young, L. M., & Bureau, M. 2007, MNRAS, 377, 1795
Dalcanton, J. J., Yoachim, P., & Bernstein, R. A. 2004, ApJ, 608, 189
de Vaucouleurs, G., de Vaucouleurs, A., Corwin, H. G., et al. 1995, VizieR Online Data Catalog, 7155, 0
Djorgovski, S., & Davis, M. 1987, ApJ, 313, 59
Dressler, A. 1980, ApJ, 236, 351
Ellison, S. L., Simard, L., Cowan, N. B., et al. 2009, MNRAS, 396, 1257
Faber, S. M., Dressler, A., Davies, R. L., Burstein, D., & Lynden-Bell, D. 1987, in Nearly Normal Galaxies. From the Planck Time to the Present, ed. S. M. Faber, 175
Fontanot, F., De Lucia, G., Monaco, P., Somerville, R. S., & Santini, P. 2009, MNRAS, 397, 1776
Fukugita, M., Nakamura, O., Turner, E. L., Helmboldt, J., & Nichol, R. C. 2004, ApJ, 601, L127
Geha, M., Blanton, M. R., Masjedi, M., & West, A. A. 2006, ApJ, 653, 240
Gómez, P. L., Nichol, R. C., Miller, C. J., et al. 2003, ApJ, 584, 210
Gu, Q., Zhao, Y., Shi, L., Peng, Z., & Luo, X. 2006, AJ, 131, 806
Gültekin, K., Richstone, D. O., Gebhardt, K., et al. 2009, ApJ, 698, 198
Haynes, M. P., & Giovanelli, R. 1984, AJ, 89, 758
Huang, S., & Gu, Q.-S. 2009, MNRAS, 398, 1651
Jorgensen, I., Franx, M., & Kjaergaard, P. 1996, MNRAS, 280, 167

Kauffmann, G., Heckman, T. M., White, S. D. M., et al. 2003a, MNRAS, 341, 33
Kauffmann, G., Heckman, T. M., Tremonti, C., et al. 2003b, MNRAS, 346, 1055
Kauffmann, G., White, S. D. M., Heckman, T. M., et al. 2004, MNRAS, 353, 713
Kaviraj, S., Schawinski, K., Devriendt, J. E. G., et al. 2007, ApJS, 173, 619
Kennicutt, R. C., Jr. 1998, ApJ, 498, 541
Larson, R. B. 1974, MNRAS, 166, 585
Le Borgne, J.-F., Bruzual, G., Pelló, R., et al. 2003, A&A, 402, 433
Lisker, T., Glatt, K., Westera, P., & Grebel, E. K. 2006, AJ, 132, 2432
Martin, C. L., & Kennicutt, R. C., Jr. 2001, ApJ, 555, 301
Mateus, A., Sodré, L., Cid Fernandes, R., et al. 2006, MNRAS, 370, 721
Morganti, R., de Zeeuw, P. T., Oosterloo, T. A., et al. 2006, MNRAS, 371, 157
Oosterloo, T., Morganti, R., Crocker, A., et al. 2010, MNRAS, 409, 500
Osterbrock, D. E. 1989, Astrophysics of Gaseous Nebulae and Active Galactic Nuclei (Mill Valley, CA: University Science Books), 422
Paturel, G., Petit, C., Prugniel, P., et al. 2003, A&A, 412, 45
Salim, S., Rich, R. M., Charlot, S., et al. 2007, ApJS, 173, 267
Sandage, A., & Visvanathan, N. 1978, ApJ, 223, 707
Schawinski, K., Khochfar, S., Kaviraj, S., et al. 2006, Nature, 442, 888
Schawinski, K., Thomas, D., Sarzi, M., et al. 2007a, MNRAS, 382, 1415
Schawinski, K., Kaviraj, S., Khochfar, S., et al. 2007b, ApJS, 173, 512
Schlegel, D. J., Finkbeiner, D. P., & Davis, M. 1998, ApJ, 500, 525
Searle, L., Sargent, W. L. W., & Bagnuolo, W. G. 1973, ApJ, 179, 427
Smith, M. W. L., Gomez, H. L., Eales, S. A., et al. 2011, arXiv:1112.1408
Strateva, I., Ivezić, Ž., Knapp, G. R., et al. 2001, AJ, 122, 1861
Suh, H., Yoon, S.-c., Jeong, H., & Yi, S. K. 2011, ApJ, 730, 110
Tremonti, C. A., Heckman, T. M., Kauffmann, G., et al. 2004, ApJ, 613, 898
Veilleux, S., Cecil, G., & Bland-Hawthorn, J. 2005, ARA&A, 43, 769
Verde, L., Oh, S. P., & Jimenez, R. 2002, MNRAS, 336, 541
Yi, S., Lee, Y.-W., Woo, J.-H., et al. 1999, ApJ, 513, 128
Yi, S. K., Yoon, S.-J., Kaviraj, S., et al. 2005, ApJ, 619, L111